Ultra-thin Optically Transparent Broadband Microwave Metamaterial Absorber Based on Indium Tin oxide

Yao Xiong
Wuhan University of Science and Technology
Fu Chen
Wuhan University of Science and Technology
Yongzhi Cheng
Wuhan University of Science and Technology
Hui Luo (luohui@wust.edu.cn)
Wuhan University of Science and Technology

Research Article

Keywords: Microwave absorption, ITO, Optical transparent, Metamaterial

Posted Date: April 22nd, 2022

DOI: https://doi.org/10.21203/rs.3.rs-1565214/v1

Abstract

A broadband metamaterial absorber (MMA) with optical transmittance property was designed to address the electromagnetic (EM) pollution in gigahertz (GHz). The proposed MMA with high optical transmittance polymethyl methacrylate (PMMA) between a periodic arrayed indium tin oxide (ITO) film and a low-resistivity ITO reflective layer. Over 90% microwave absorbance can be achieved in the frequency range of 6-17.8 GHz and three distinct absorption peaks can be found in the reflection spectrum. The results also show wide-angular stability, good polarization insensitiveness, and optical transmittance properties. The microwave attenuation mechanisms of the proposed MMA were investigated using surface current distribution and power loss density. The excellent microwave absorption and optical transmittance properties indicate that the designed MMA has strong potential for developing optical transmittance microwave absorption windows and devices.

1. Introduction

Electromagnetic (EM) pollution has become a serious problem with the wide application of the microwave radio technology, which poses a threat to human health and precision devices.[1–4] Excellent microwave absorbing materials, which can convert EM wave energy into heat energy and block the propagation of EM waves, has become a dramatic subject for decades. .[5, 6] Remarkable efforts have been devoted to design and fabricate the MAs, and promoted the rapid development of microwave absorption technology in recent years.[7–9] Salisbury Screen consisting of a single equally distribution resistive sheet and a perfectly metallic surface is a quarter wavelength resonant narrowband absorber.[10] The limitation of the Salisbury Screen is that only EM waves near the resonant frequency can be absorbed. The Jaumann absorber expands the absorption bandwidth by increasing the number of resistive sheets, nevertheless, increasing the manufacturing difficulty and the cost of the absorber.[11, 12] In addition, a variety of absorbers, such as Dallenbach absorbers and pyramidal absorbers, also have been developed to broaden the absorption bandwidth. Such as it is, the absence of the volume, rigidity, and optical transparency properties of the absorbers limited their practical application.[13–17]

Metamaterial with artificially designed sub-wavelength structures exhibit extraordinary EM properties compared with natural materials, and have been widely applied for EM wave absorption from microwave to optical frequencies in recent years.[18–21] Abundant efforts have been made to push forward the development of MMAs since the first perfect MMA was proposed by Landy et al.[22] MMAs caused extensive concern for the near-perfect absorption at some specific frequencies. Various MMAs were designed and manufactured to achieve broadband absorption, light weight and robust angular performance, and optical transparent MMAs were manufactured to meet some special applicable scene.[23–26] Compared with traditional absorbers, MMAs can regulate their relative permittivity and permeability by changing parameters of structure and materials properties. Metamaterials can manipulate EM waves flexibly, which makes it possible to improve the microwave absorption performance.[27–30] Recently, optical transmittance property has become an important index of the

absorber because of the application and rapid development of MMAs for EM protection and intelligent stealth in the field of aviation. However, majority MMAs are composed of opaque materials, which impeded their application in some scenarios requiring optical transparency. Various routes have been attempted to achieve optically transparent absorbers. For example, Zhang et al. designed a wind-mill shaped MMA with an efficient microwave absorption (over 90%) from 8.3 to 17.4 GHz with around 77% optical transmittance.[31] Hu et al. developed a broadband microwave MMA with standing-up closed-ring resonators, achieving above 85% absorbance from 5.5–19.7 and 22.5-27.5GHz with an optical transmittance around 82%.[32] Zhang et al. demonstrated an actively tunable MMA with a water-based substrate, polymethyl methacrylate (PMMA), distilled water and ITO films, achieving absorbance over 90% within 5.8–16.2 GHz, and 70.18% optical transmittance.[33] Other design schemes, including multilayer transparent resistive film and aluminum wire grids, which has great advantages in working bandwidth, but the multilayer structure inevitably reduces the overall transmittance of the absorber. [26, 34, 35] The absorption bandwidth of aluminum wire grids transparent absorber is limited for its operating bandwidth strongly depends on the structure of the composite resonance. In addition, the complexity, high cost and effective absorption bandwidth of these methods limit their practical application. Resistive film (ITO) with the characteristics of high efficiency absorption, easy fabrication and high optical transmittance make it a good choice for the fabrication of optical transparent absorbers.

Herein, an MMA with high optical transparency and broadband microwave absorption based on resistance loss and multi-resonance attenuation characteristics was fabricated. The S-parameter obtained via full-wave simulations show that the proposed structure has three strong resonant peaks, which strongly depend on the structural parameters of the MMA. The realization of broadband absorption benefits from the reasonable adjustment of multi-resonance frequency and the ohmic loss of the proposed MMA structure. The designed MMA is a multilayer structure, including polyethylene terephthalate (PET) and polymethyl methacrylate (PMMA) dielectric substrate and resistance film ITO. Periodic array and low resistance ITO on the PET substrate are used at the top layer and the bottom layer, respectively. The overall structure can simultaneously achieve high transmittance at the range of visible frequency for the high optical transmittance of ITO-PET and PMMA. The designed MMA ensures over 90% absorption within 6-17.8 GHz for both transverse electric (TE) and transverse magnetic (TM) mode waves under normal incidence, and about 57% optical transmittance in the visible range with the total thickness of the designed MMA is 3.55 mm. Simultaneously, EM absorption performance can still be maintained well for TE- and TM-polarized waves when the incident angle is less than 45°. The consistency between the experimental results and the simulation results indicates that the designed optical transparent MMA can be used as a reliable candidate product in the transparent window of optical EM wave shielding.

2. Theoretical Simulation And Analysis

The designed optical transparent MMA based on resistance loss and multi-resonance characteristics is shown in Fig. 1(a), consisting a periodic arrayed ITO-PET on the top layer, PMMA plate and low resistance

ITO-PET reflective backplane placed in the middle and bottom layers in sequence. The top and side view of the MMA unit-cell structure are illustrated in Fig. 1(b) and Fig. 1(c), respectively. All the constituent materials have prosperous optical transparency, which ensures the overall structure possesses distinguished optical transmittance properties. Multiple resonance modes are introduced into the periodic arrayed ITO-PET to generate different EM resonances to ensure the broadband microwave absorption. Excellent microwave absorption under different polarization modes can be achieved because of the proposed MMA with four-fold symmetry. In this work, both of the upper and lower surfaces were composed of ITO-PET film with commercial availability. The dielectric constants of PMMA and PET are 2.25(1-j0.001) and 3.0(1-j0.06), respectively.

The numerical simulation for the unit-cell structure of the MMA was performed by the CST Microwave Studio 2016. The boundary conditions of the unit-cell structure were set to periodic boundary condition and add space in x-y plane and z direction respectively. The absorbance of the MMA in the frequency range of 2–18 GHz can be calculated by S-parameter. The relationship among absorbance, reflectance and transmittance is as follows[36]:

$$R(\omega) = |S_{11}|^2$$

1

$$T(\omega) = |S_{21}|^2$$

2

$$A(\omega) = 1 - R(\omega) - T(\omega)$$

3

where $A(\omega)$, $R(\omega)$ and $T(\omega)$ are energy absorbance, reflectance and transmittance, respectively. The bottom ITO film with low resistance can be regarded as a metal backplane with good conductivity, which ensuring the incident EM wave was almost reflected. In consequence, the transmittance can be neglected, and the absorbance is approximately equal to[36]:

$$A(\omega) = 1 - R(\omega)$$

4

To clarify the process of our proposed structure for ideal absorption bandwidth, the intermediate configuration process of the absorber is analyzed, as shown in Fig. 2. An absorption peak appears at 8.4 GHz, and the absorbance is less than 90% in the whole simulation frequency range when there is only the cross structure on the top layer. The bandwidth was enhanced by incorporating the cross ring in the structure, and the resonant frequency moves to lower frequency. Finally,, the windmill structure was integrated in the final design, which further enhances the level of absorbance.

Microwave absorption bandwidth of the MMA is a key factor to evaluate the microwave absorption performance, which can be regulated by changing the geometric structure and composition materials. To obtain excellent microwave absorption performance, the geometric parameters of the proposed structure are optimized and the absorbance change with the structural parameters is shown in Figs. 3(a-d). With the increase of PMMA thickness t_d, the absorption performance of the low-frequency part becomes better, while the high-frequency part becomes weaker, and the overall absorption bandwidth becomes narrower. The proposed MMA obtains the best absorbance when the PMMA thickness td equals 3.2 mm. In the upper ITO layer, the absorbance at low frequency becomes worse with the increase of g_1. The MMA shows the best absorption effect when g_1 is 0.2 mm. It can be seen from Fig. 3(c) that the change of the resistance R_{s2} value of the reflection backplane has little effect on the absorbance, which means that ITO resistance can have a certain error in the actual production of the bottom. The relationship between the microwave absorption bandwidth and the value of the top layer surface resistance (R_{s1}) is shown in Fig. 3(d). The absorbance shows three sharp and discontinuous absorption peaks when the value of top layer surface resistance is 45Ω/sq. As the R_{s1} value increases to 65Ω/sq, the three absorption peaks become mild and continuous. Therefore, the enhanced effective absorption bandwidth maybe due to the improved impedance matching. In the resonant circuit, the quality factor Q of the circuit is closely related to the characteristics of the resonant peak. The higher the Q value, the sharper the resonant curve. In the designed structure, with the increase of R_{s1}, the quality factor Q gradually decreases, and the three resonant peaks tend to be continuous. The relation formula between quality factor and bandwidth is[30]:

$$Q = \omega_0 \times \frac{P_T}{P_L} = \frac{f_0}{\Delta f}$$

5

where P_T and P_L are the stored and consumed energy, ω_0 and f_0 are the resonant frequencies and Δf is the absorption bandwidth. It can be seen from the absorbance curve that the resonant frequency f_0 of the structure is constant, and the decrease of Q factor will increase the absorption bandwidth of the MMA. The ITO film with high resistance can increase the value of P_L and enables the fusion of multiple absorption peaks to achieve broadband absorption. The optimized geometric parameters of the proposed unit-cell structure are as follows: p = 16.6 mm, w_1 = 4 mm, w_2 = 11.2 mm, w_3 = 2 mm, w_4 = 5.4 mm, g_1 = 0.2 mm, g_2 = 0.1 mm, d_1 = 1.3 mm, d_2 = 4.6 mm, t_p=0.175 mm and t_d=3.2 mm. The resistance of the top ITO pattern layer and the bottom ITO reflective backplane are R_{S1}=55 Ω/sq and R_{S2}=6 Ω/sq, respectively.

The microwave absorbance of normal incident transverse electric (TE) wave along the surface of MMA is shown in Fig. 4(a). There are three absorption peaks at about 7 GHz, 11.4 GHz and 16.8 GHz, respectively. The absorption peaks at 7 GHz and 16.8 GHz are moderate and near perfect absorption is realized at 11.4 GHz. The MMA achieves effective absorption (90% absorbance) in the frequency range of 6.0-17.8 GHz, exhibiting a relative bandwidth of 99.2% with a center frequency of 11.9 GHz. To explain the response of the proposed MMA to the incident EM waves, the homogenization algorithm was used to retrieve the

relative permittivity (ϵ) and relative permeability (μ) of the structure. The S-parameters S_{11} and S_{21} are necessary according to the equivalent medium theory to successfully retrieve the EM parameters of the MMA structure. Since the reflective backplane of the proposed transparent MMA is a whole piece of ITO film, in order to obtain S_{21}, we dig four square holes at four corners of the ITO backplane of the unit-cell.[37] The calculation formulas of equivalent relative impedance (z), equivalent permittivity (ϵ) and permeability (μ) can be expressed as[38]:

$$z = \pm \sqrt{\frac{(1+S_{11})^2 - S_{21}^2}{(1-S_{11})^2 - S_{21}^2}}$$

6

$$\varepsilon = \frac{n}{z}$$

7

$$\mu = nz$$

8

The calculation formula of relative refractive index n is[38]:

$$n = \pm \frac{1}{kd}\cos^{-1}\left[\frac{1}{2S_{21}}\left(1 - S_{11}^2 + S_{21}^2\right) + 2m\pi\right]$$

9

and

$$k = \frac{2\pi\lambda}{c}$$

10

where d is the overall thickness of the proposed transparent MMA, m is any integer, c is the propagation velocity of wave in vacuum, and λ is wavelength. The S-parameter is obtained by EM simulation, and combined with Formulas (6)-(10), the relative EM parameters of the proposed MMA structure are shown in Figs. 4(b-d). Figure 4(b) shows the normalized input impedance (z) obtained in the frequency range of 4–18 GHz. The value of the real part of z is almost close to 1 besides one peak at about 14 GHz, and the imaginary part of z is around 0, indicating that the designed MMA meets the basic principle of impedance matching and the incident EM waves would enter into the absorber. Almost perfect impedance matching

is implemented at 11.4 GHz, which is also consistent with the ultra-strong absorption band of incident EM waves at this frequency. Figure 4(c) and Fig. 4(d) show the curves of the real and imaginary parts of the relative permittivity and permeability of the proposed MMA. In the working frequency range (6.0-17.8GHz) of the MMA, the imaginary part of the relative permittivity varies from 0 to 20, and decreases with the increase of frequency, which indicates that the electrical loss decreases with the increase of frequency. The imaginary part of relative permeability varies from 0 to 15 in the working range of the MMA, and the response to EM waves at 6 GHz and 14 GHz is magnetic resonance. The relative EM parameters prove that electric resonance and magnetic resonance coexist in the proposed transparent MMA.

In MMAs, the augment of absorption intensity and absorption bandwidth is usually caused by the excited electric and magnetic resonance. Electric and magnetic resonance are closely related to the current flow direction of the top and bottom layers. To further understand the microwave attenuation mechanisms of the designed MMA, the electric current distributions on the top and bottom layers at the three resonant frequencies were investigated under normal incidence, as shown in Fig. 5. The excited electric current on the top layer induced by the incident EM waves is mainly concentrated at the corner of the internal cross, and the current direction is along the positive direction of x axis tt 7 GHz, as shown in Fig. 5(a). As shown in Fig. 5(d), the induced current on the bottom plate is along the negative direction of x-axis, which is opposite to the top layer, proving the near-field coupling between the top and the reflective backplane led to the magnetic resonance loss. Except for the opposite direction of the excited current, the induced current distribution at 11.4 GHz and 16.8 GHz are similar, which mainly concentrated in the windmill structure along the x-axis direction of the branch, as shown in Fig. 5(b) and Fig. 5(c). As shown in Fig. 5(e) and Fig. 5(f), the current on the backplane is anti-parallel to the current on the top layer at 11.4 GHz and 16.8 GHz which indicating that magnetic resonance loss occur at 11.4 GHz and 16.8 GHz,. As a result, the magnetic resonance makes the absorption performance of the MMA significantly enhanced. It also can be found that the current intensity at the top surface are far stronger than the bottom layer, indicating that the magnetic resonance maybe not the main reason for EM energy attenuation. The strong EM energy maybe caused by the resistance loss. By comparing Figs. 5(a)-(c) and Figs. 5(g)-(h), it is found that the EM waves energy loss is highly consistent with the location of the induced current concentration of ITO layers. This is because the ITO layers has a certain resistance, which will produce significant ohmic loss under the action of the induced current, according to[39]:

$$P_{loss} = I^2 R_{ITO}$$

11

where I is the induced current intensity and R_{ITO} is the sheet resistance of the top ITO film.

Microwave absorption performance at different incident angles were discussed for most EM waves are not vertically incident on the absorber surface in practical applications. The absorption performance of the MMA with different incident angles under TE and TM polarization are shown in Fig. 6. For TE polarization and TM polarization, the microwave absorption performance of the MMA gradually

deteriorates as the incident angle of EM waves increases from 0° to 60°. Compared with TE polarization, the microwave absorption performance under TM polarization at different incident angles is higher, indicating that the angle stability is better for TM polarization. In the case of TE polarized mode (Fig. 6(a)), when the incident angle is less than 30°, over 90% absorption can be still maintained. When the incident angle is greater than 45°, the absorption performance of the proposed MMA is greatly reduced. The main factor for the decrease of the absorbance is that the magnetic flux through the multilayer structure decreases with the increase of the incident angle, leading to the decrease of the circulating current of the ITO surface and the impedance mismatching. In the case of TM polarized mode (see Fig. 6(b)), when the incident angle is 0° – 45°, over 90% absorbance can still be maintained. Over85% absorbance can still be guaranteed when the incident angle reaches 60° under TM polarized mode, which is due to the magnetic field is parallel to the surface in TM polarization mode and the EM wave absorption is mainly caused by the magnetic resonance. [40]

3. Experimental Verification

To certify the designed transparent MMA in this work has broadband absorption and high transmittance properties in the frequency range of 6-17.8 GHz, we fabricated the sample with the overall size of 200×200 mm^2 consisting of 12×12-unit cells (Fig. 7(a)). The top-layer ITO resistance film is patterned by laser micro-precision machining technology. Then the patterned ITO-PET layer, PMMA substrate and ITO-PET backplane were bonded together by high transparent optical adhesive. Here, the thickness of PMMA medium is 3.0 mm in the actual sample due to the limitation of industrial production. The prepared samples were measured in a microwave anechoic chamber using free space method. The reflectance measurement equipment of transparent absorber includes vector network analyzer (Agilent N5244A) and a pair of broadband antennas (the measured spectrum range is 2–18 GHz). The curves of normal incident plane wave reflection versus frequency obtained by measurement and simulation are shown in Fig. 7(b). The measured data and simulation data show that the measured absorbance curve is basically consistent with the simulated one in the frequency range of 6–13 GHz. Due to the limitation of fabrication process, it is difficult to precisely control the resistance of ITO film at a certain value, which will greatly affect the impedance matching characteristics of the MMA. Other factors that affect the measurement results include the gap between the materials of each layer, the glue adhered to each layer and the measurement environment. Visible light photometer (shimadzu uv3600plus) with high sensitivity is used to measure the optical transparency coefficient of the sample. In the wavelength range of 400–800 nm, the visible light transmittance coefficient curve is shown in Fig. 6(c). The measurement results show that the average transmittance of the prepared sample is about 57%, which has a certain gap with our target transmittance. Among the materials that compose the absorber sample, the average transmittance of PMMA medium is about 98%, and the key factor affecting the overall transmittance of the absorber sample is ITO-PET. However, the transmittance of ITO-PET produced by different manufacturers is different, so it is difficult to select the best material for the MMA sample. And in the whole ITO-PET etching, ITO-PET surface has certain wear, these factors directly lead to the overall

transmittance decreased. The transparent MMA is placed on the emblem of Wuhan University of Science and Technology (Fig. 7(d)), which proves the optical transparency of the model.

Compare the experimental data of reported transparent MMA, our design has some advantages in absorbing bandwidth and the total thickness, as shown in Table 1.

Table 1: Comparison with other broadband transparent MMA

Absorber	absorption band >90%	Relative bandwidth[a]	thickness	Optical transmittance
Ref.31	8.3-17.4GHz	70.8%	3.85mm	~77%
Ref.6	5.8-17.0GHz	98.24%	6mm	~
Ref.33	5.8-16.2GHz	94.5%	4.15mm	~70.18%
Ref.32	5.5-19.7GHz and 22.5-27.5GHz	113.6%	5.5mm	~82%
Ref.34	6.1-22.1GHz	112.7%	3.8mm	~86%
This work	6.7-14.1GHz	71.2%	3.55mm	~57%

[a] The calculation method of the relative absorption bandwidth is defined as $RB = 100\% * (f_{max} - f_{min}) / (f_{max} + f_{min}) / 2$, where f_{min} and f_{max} are the lowest and highest frequencies of the effective absorbing band, respectively.

In engineering applications, transparent MMAs are often required to be flexible. To achieve the overall bending and transparency of the absorber, the non-bending medium PMMA material is replaced by the bending and transparent medium PVC material. It should be pointed out that the average transmittance of PVC (the average transmittance is about 90%) is smaller than that of PMMA (the average transmittance is about 95%), so the selection of PVC to make flexible transparent absorber will reduce the overall transmittance of the absorber. The dielectric constant of PVC material is 2.45(1-j0.012). Figure 8 shows the absorption curves of the absorber using PMMA medium and PVC medium. The curves of the two groups of simulation data are consistent, which proves that it is feasible to choose flexible PVC material as a transparent component to realize a flexible transparent MMA.

4. Conclusion

In conclusion, A broadband microwave MMA with high visible transmittance was designed and fabricated. Incident angle stability and polarization insensitive for TE-polarized and TM-polarized waves are considered as additional advantages in practical applications. Through the design and optimization

of MMA structure, over 90% absorbance can be achieved at the frequency range of 6-17.8 GHz. In addition, since the materials of the MMA are all highly transparent, the overall transmittance can reach 57%. Compared with other transparent MMAs, our proposed absorber has certain advantages in overall thickness (only 3.55mm) and absorption bandwidth over 90% absorbance bandwidth is 11.8GHz. The experimental results are consistent with the simulation results. This transparent broadband MMA can be used as an optical window for wide applications in aviation, medical and civil fields.

References

1. Liu, J.; Zhang, H. B.; Sun, R.; Liu, Y.; Liu, Z.; Zhou, A.; Yu, Z. Z., Hydrophobic, Flexible, and Lightweight MXene Foams for High-Performance Electromagnetic-Interference Shielding. Adv Mater **2017**, *29* (38).
2. Shahzad, F.; Alhabeb, M.; Hatter, C. B.; Anasori, B.; Hong, S. M.; Koo, C. M.; Gogotsi, Y. J. S., Electromagnetic interference shielding with 2D transition metal carbides (MXenes). 2016, *353* (6304), 1137–1140.
3. Frey, A. H. J. E. h. p., Headaches from cellular telephones: are they real and what are the implications? 1998, *106* (3), 101–103.
4. Zhang, X.; Ji, G.; Liu, W.; Quan, B.; Liang, X.; Shang, C.; Cheng, Y.; Du, Y., Thermal conversion of an Fe(3)O(4)@metal-organic framework: a new method for an efficient Fe-Co/nanoporous carbon microwave absorbing material. Nanoscale 2015, *7* (30), 12932–42.
5. Cheng, Y.; Luo, H.; Chen, F., Broadband metamaterial microwave absorber based on asymmetric sectional resonator structures. Journal of Applied Physics 2020, *127* (21).
6. Sheokand, H.; Singh, G.; Ghosh, S.; Ramkumar, J.; Ramakrishna, S. A.; Srivastava, K. V., An Optically Transparent Broadband Microwave Absorber Using Interdigital Capacitance. IEEE Antennas and Wireless Propagation Letters 2019, *18* (1), 113–117.
7. Kong, L. B.; Li, Z. W.; Liu, L.; Huang, R.; Abshinova, M.; Yang, Z. H.; Tang, C. B.; Tan, P. K.; Deng, C. R.; Matitsine, S., Recent progress in some composite materials and structures for specific electromagnetic applications. International Materials Reviews 2013, *58* (4), 203–259.
8. Vinayasree, S.; Soloman, M. A.; Sunny, V.; Mohanan, P.; Kurian, P.; Anantharaman, M. R., A microwave absorber based on strontium ferrite–carbon black–nitrile rubber for S and X-band applications. Composites Science and Technology 2013, *82*, 69–75.
9. Ranjan, P.; Choubey, A.; Mahto, S. K., A novel approach for optimal design of multilayer wideband microwave absorber using wind driven optimization technique. AEU - International Journal of Electronics and Communications 2018, *83*, 81–87.
10. Salisbury, W. W., Absorbent body for electromagnetic waves. Google Patents: 1952.
11. Du Toit, L. J. J. I. A.; Magazine, P., The design of Jauman absorbers. 1994, *36* (6), 17–25.
12. Du Toit, L. J.; Cloete, J. H. J. I. t. o. m. t.; techniques, Electric screen Jauman absorber design algorithms. 1996, *44* (12), 2238–2245.

13. Takizawa, K.; Hashimoto, O. J. I. t. o. m. t.; techniques, Transparent wave absorber using resistive thin film at V-band frequency. 1999, *47* (7), 1137–1141.
14. Wu, B.; Tuncer, H. M.; Naeem, M.; Yang, B.; Cole, M. T.; Milne, W. I.; Hao, Y., Experimental demonstration of a transparent graphene millimetre wave absorber with 28% fractional bandwidth at 140 GHz. Sci Rep 2014, *4*, 4130.
15. Batrakov, K.; Kuzhir, P.; Maksimenko, S.; Paddubskaya, A.; Voronovich, S.; Lambin, P.; Kaplas, T.; Svirko, Y., Flexible transparent graphene/polymer multilayers for efficient electromagnetic field absorption. Sci Rep 2014, *4*, 7191.
16. Chambers, B.; Tennant, A. In *Active Dallenbach radar absorber*, 2006 IEEE Antennas and Propagation Society International Symposium, IEEE: 2006; pp 381–384.
17. Nornikman, H.; Ahmad, B. H.; Aziz, M. Z. A. A.; Abd Malek, M. F. B.; Imran, H.; Othman, A. R. J. P. I. E. R., Study and simulation of an edge couple split ring resonator (EC-SRR) on truncated pyramidal microwave absorber. 2012, *127*, 319–334.
18. Alù, A., Mantle cloak: Invisibility induced by a surface. Physical Review B **2009**, *80* (24).
19. Valentine, J.; Zhang, S.; Zentgraf, T.; Ulin-Avila, E.; Genov, D. A.; Bartal, G.; Zhang, X., Three-dimensional optical metamaterial with a negative refractive index. Nature 2008, *455* (7211), 376-U32.
20. Pendry, J. B. J. P. r. l., Negative refraction makes a perfect lens. 2000, *85* (18), 3966.
21. Alù, A.; Engheta, N., Plasmonic and metamaterial cloaking: physical mechanisms and potentials. Journal of Optics A: Pure and Applied Optics 2008, *10* (9).
22. Landy, N. I.; Sajuyigbe, S.; Mock, J. J.; Smith, D. R.; Padilla, W. J., Perfect metamaterial absorber. Phys Rev Lett **2008**, *100* (20), 207402.
23. Kazemzadeh, A.; Karlsson, A., Multilayered Wideband Absorbers for Oblique Angle of Incidence. IEEE Transactions on Antennas and Propagation **2010**, *58* (11), 3637–3646.
24. Sun, L.; Cheng, H.; Zhou, Y.; Wang, J. J. O. e., Broadband metamaterial absorber based on coupling resistive frequency selective surface. 2012, *20* (4), 4675–4680.
25. Liu, X.; Gao, J.; Yang, H.; Liu, H.; Wang, X.; Shen, Z., Near-Infrared Absorption Enhancement Mechanism Investigations of Deep-Trench Silicon Microstructures Covered with Gold Films. Plasmonics **2015**, *11* (4), 1019–1024.
26. Jang, T.; Youn, H.; Shin, Y. J.; Guo, L. J., Transparent and Flexible Polarization-Independent Microwave Broadband Absorber. ACS Photonics 2014, *1* (3), 279–284.
27. Zhou, F.; Bao, Y.; Cao, W.; Stuart, C. T.; Gu, J.; Zhang, W.; Sun, C., Hiding a realistic object using a broadband terahertz invisibility cloak. Sci Rep 2011, *1*, 78.
28. Chen, P.-Y.; Alu, A. J. A. n., Atomically thin surface cloak using graphene monolayers. 2011, *5* (7), 5855–5863.
29. Tao, H.; Landy, N. I.; Bingham, C. M.; Zhang, X.; Averitt, R. D.; Padilla, W. J. J. O. e., A metamaterial absorber for the terahertz regime: design, fabrication and characterization. 2008, *16* (10), 7181–7188.

30. Huang, L.; Chen, X.; Mühlenbernd, H.; Zhang, H.; Chen, S.; Bai, B.; Tan, Q.; Jin, G.; Cheah, K.-W.; Qiu, C.-W.; Li, J.; Zentgraf, T.; Zhang, S., Three-dimensional optical holography using a plasmonic metasurface. *Nature Communications* 2013, *4* (1).
31. Zhang, C.; Cheng, Q.; Yang, J.; Zhao, J.; Cui, T. J., Broadband metamaterial for optical transparency and microwave absorption. Applied Physics Letters **2017**, *110* (14).
32. Hu, D.; Cao, J.; Li, W.; Zhang, C.; Wu, T.; Li, Q.; Chen, Z.; Wang, Y.; Guan, J., Optically Transparent Broadband Microwave Absorption Metamaterial By Standing-Up Closed-Ring Resonators. Advanced Optical Materials **2017**, *5* (13).
33. Zhang, Y.; Dong, H.; Mou, N.; Li, H.; Yao, X.; Zhang, L., Tunable and transparent broadband metamaterial absorber with water-based substrate for optical window applications. Nanoscale 2021, *13* (16), 7831–7837.
34. Li, L.; Xi, R.; Liu, H.; Lv, Z., Broadband polarization-independent and low-profile optically transparent metamaterial absorber. Applied Physics Express 2018, *11* (5).
35. Yang, Y.; Chen, S.; Li, W.; Li, P.; Ma, J.; Li, B.; Zhao, X.; Ju, Z.; Chang, H.; Xiao, L.; Xu, H.; Liu, Y., Reduced Graphene Oxide Conformally Wrapped Silver Nanowire Networks for Flexible Transparent Heating and Electromagnetic Interference Shielding. ACS Nano 2020, *14* (7), 8754–8765.
36. Ma, Y.; Wang, J.; Shi, L.; Xue, S.; Ran, Y.; Li, J.; Liu, Y., Ultra-wideband, optically transparent, and flexible microwave metasurface absorber. Optical Materials Express 2021, *11* (7).
37. Wang, Q.; Cheng, Y., Compact and low-frequency broadband microwave metamaterial absorber based on meander wire structure loaded resistors. AEU - International Journal of Electronics and Communications 2020, 120.
38. Smith, D.; Vier, D.; Koschny, T.; Soukoulis, C. J. P. r. E., Electromagnetic parameter retrieval from inhomogeneous metamaterials. 2005, *71* (3), 036617.
39. Gao, Z.; Xu, C.; Tian, X.; Wang, J.; Tian, C.; Yang, B.; Qu, S.; Fan, Q., Ultra-wideband flexible transparent metamaterial with wide-angle microwave absorption and low infrared emissivity. Opt Express 2021, *29* (14), 22108–22116.
40. Cheng, Y.; Yang, H.; Cheng, Z.; Wu, N. J. A. P. A., Perfect metamaterial absorber based on a split-ring-cross resonator. 2011, *102* (1), 99–103.

Figures

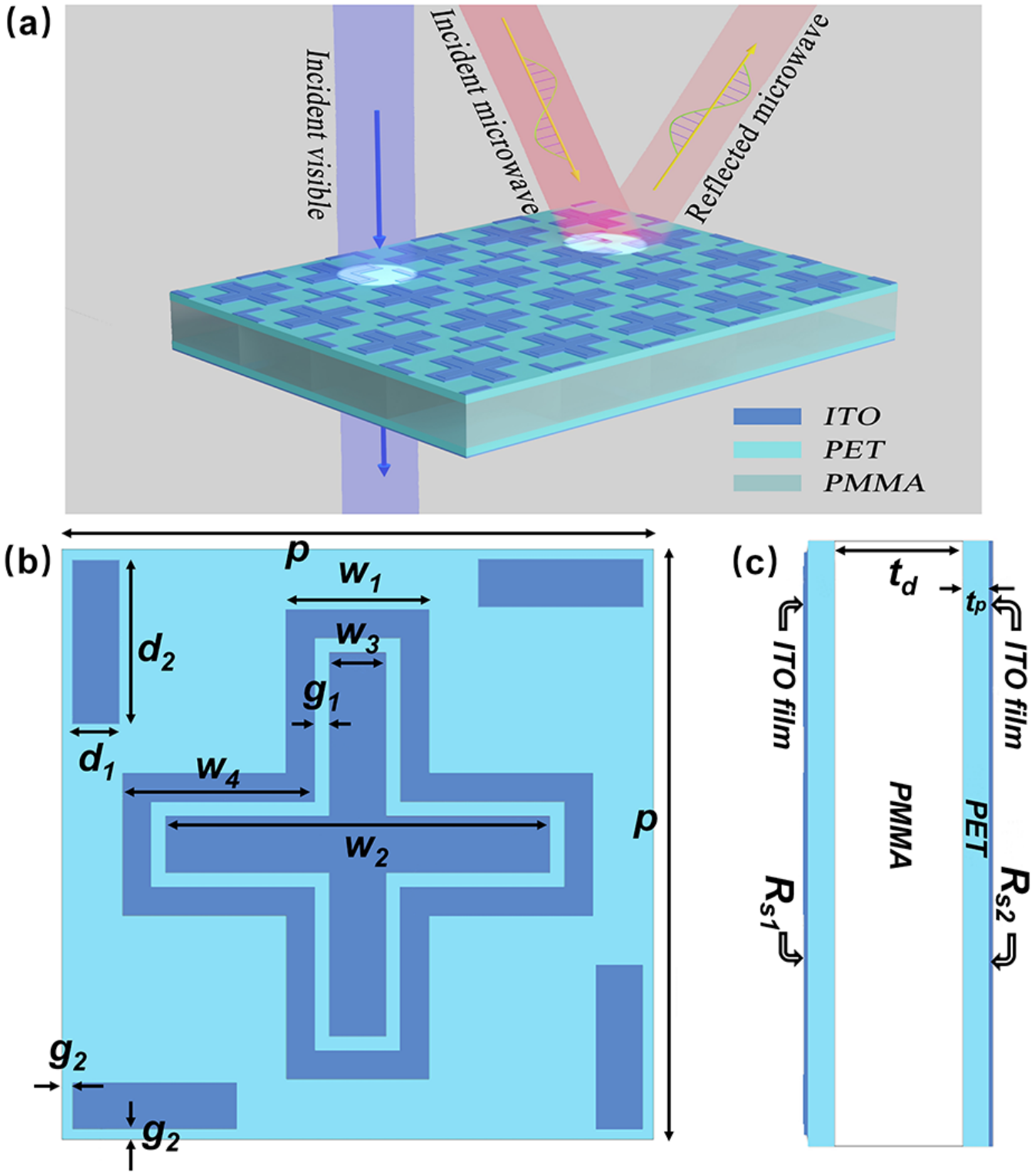

Figure 1

(a) Unit cell of the proposed MMA, (b) top and (c) lattice view.

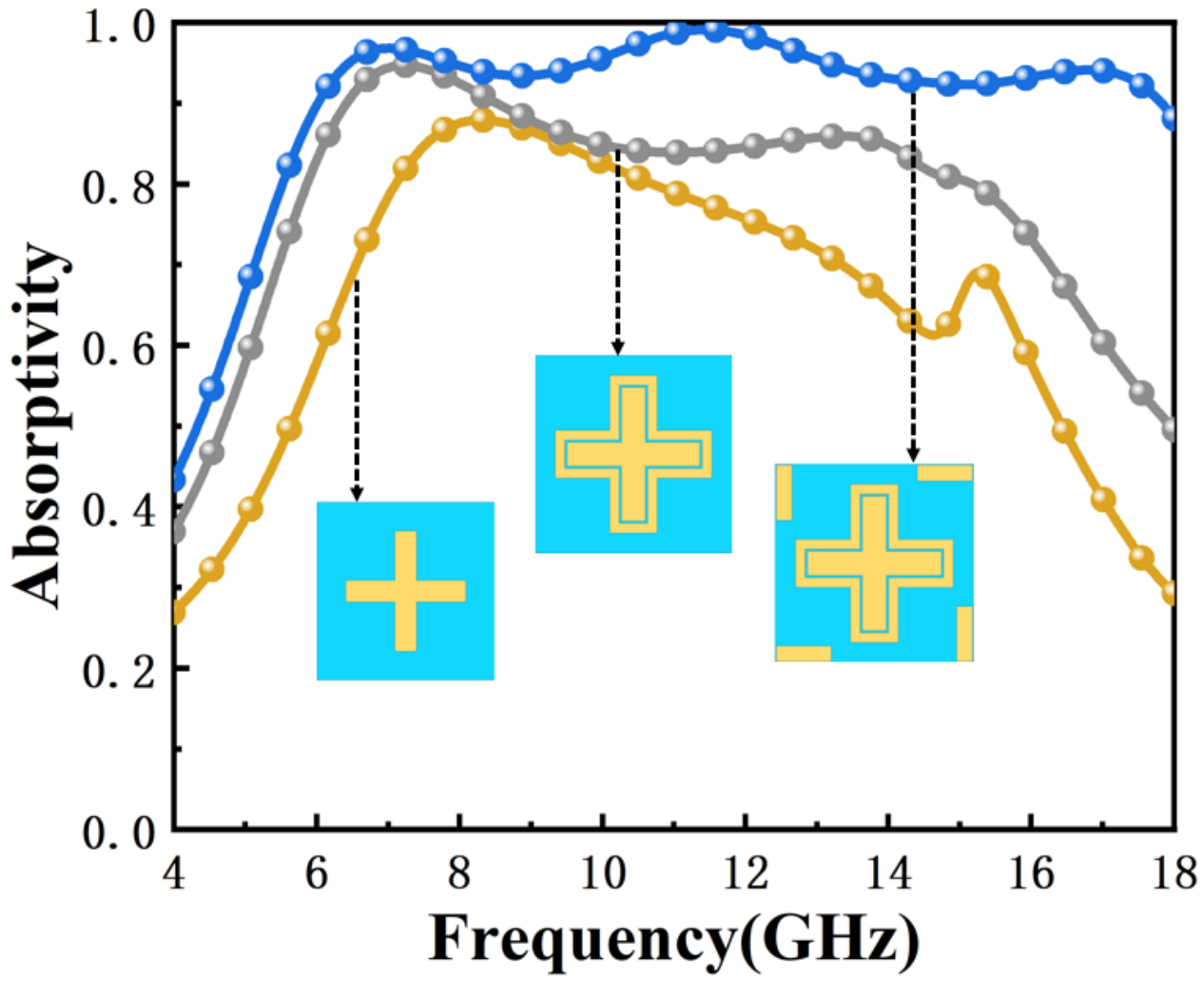

Figure 2

Simulated the absorbance curve of the designed absorber for the intermediate configuration process.

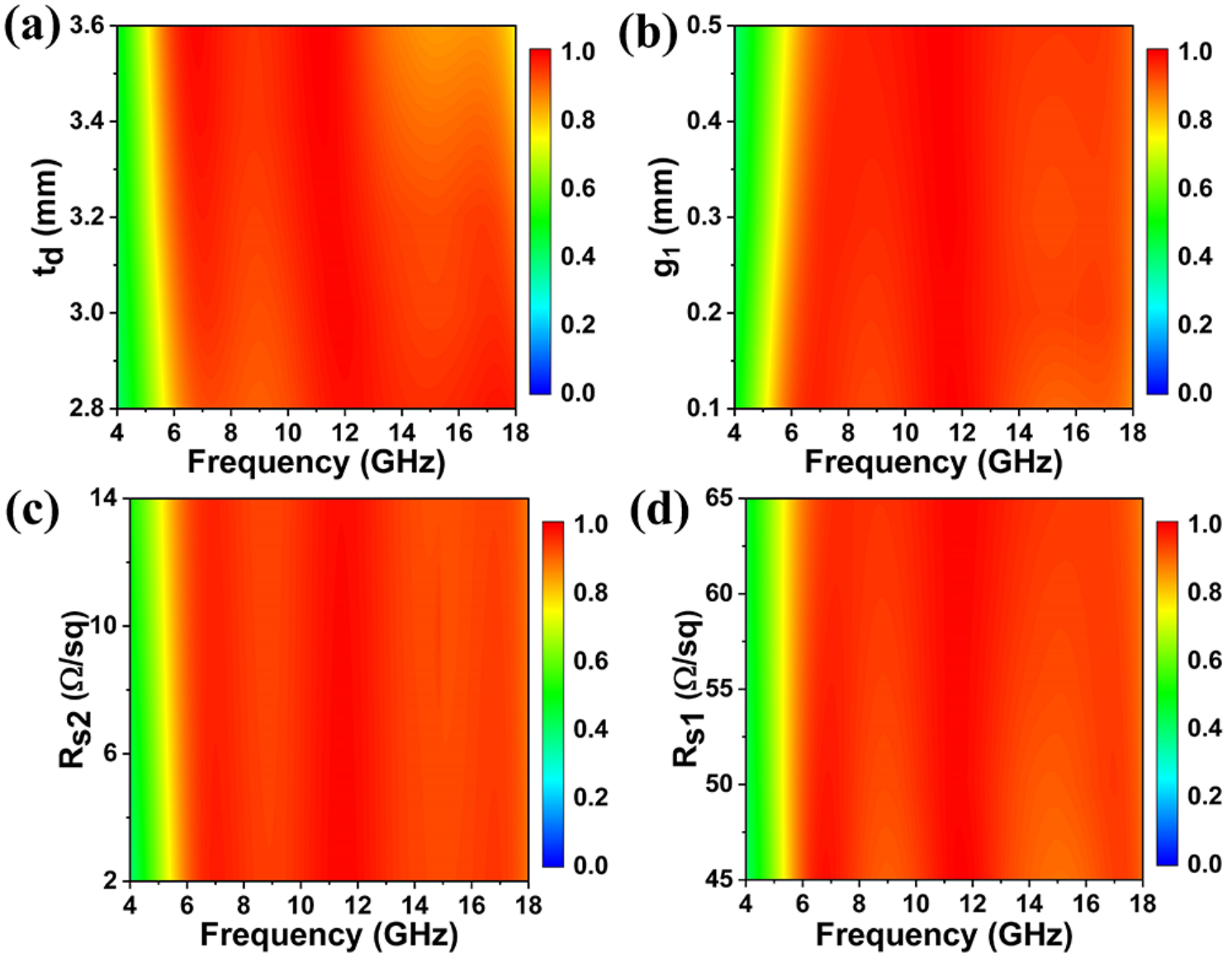

Figure 3

Simulated absorbance with different structural parameters: (a) PMMA thickness t_d, (b) gap g_1, (c) resistance R_{s2} and (d) R_{s1}.

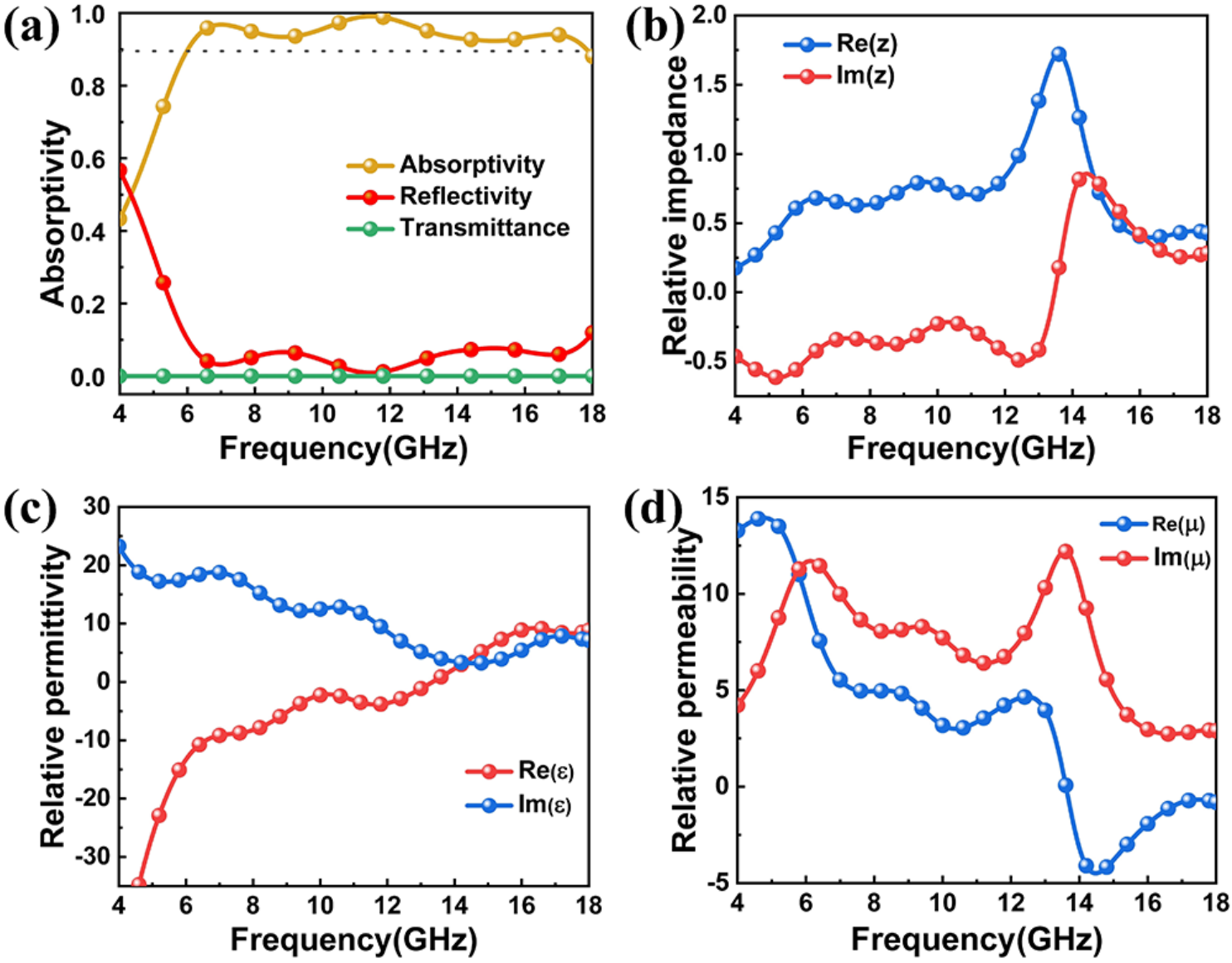

Figure 4

(a) Absorbance, reflectance and transmittance of the proposed MMA (b) normalized input impedance of the MMA (c) retrieved relative permittivity and (d) retrieved relative permeability

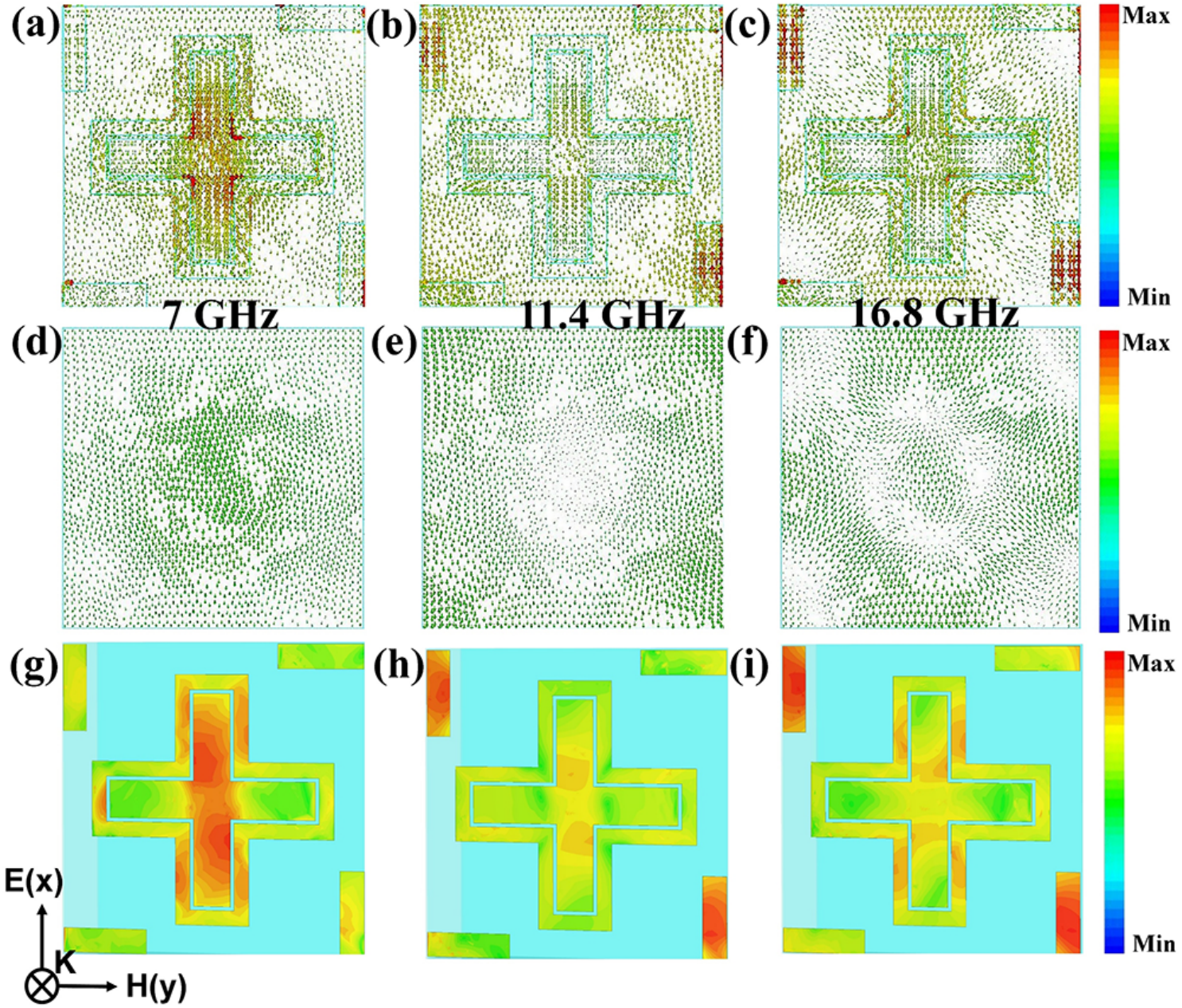

Figure 5

(a-c) Top-layer surface current, (d-f) bottom surface current and (g-i) power loss density of the proposed MMA at 7 GHz, 11.4 GHz and 16.8 GHz.

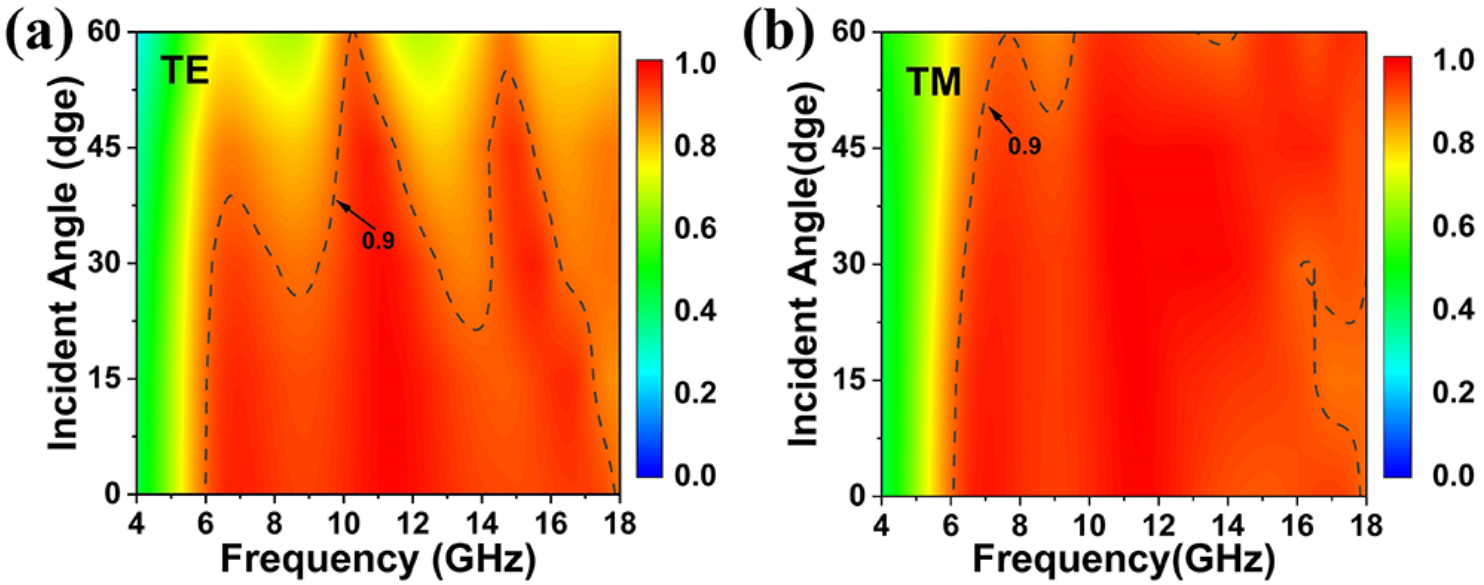

Figure 6

Simulated absorbance of the proposed MMA with different incident angles for (a) TE-polarized wave and (b) TM-polarized wave.

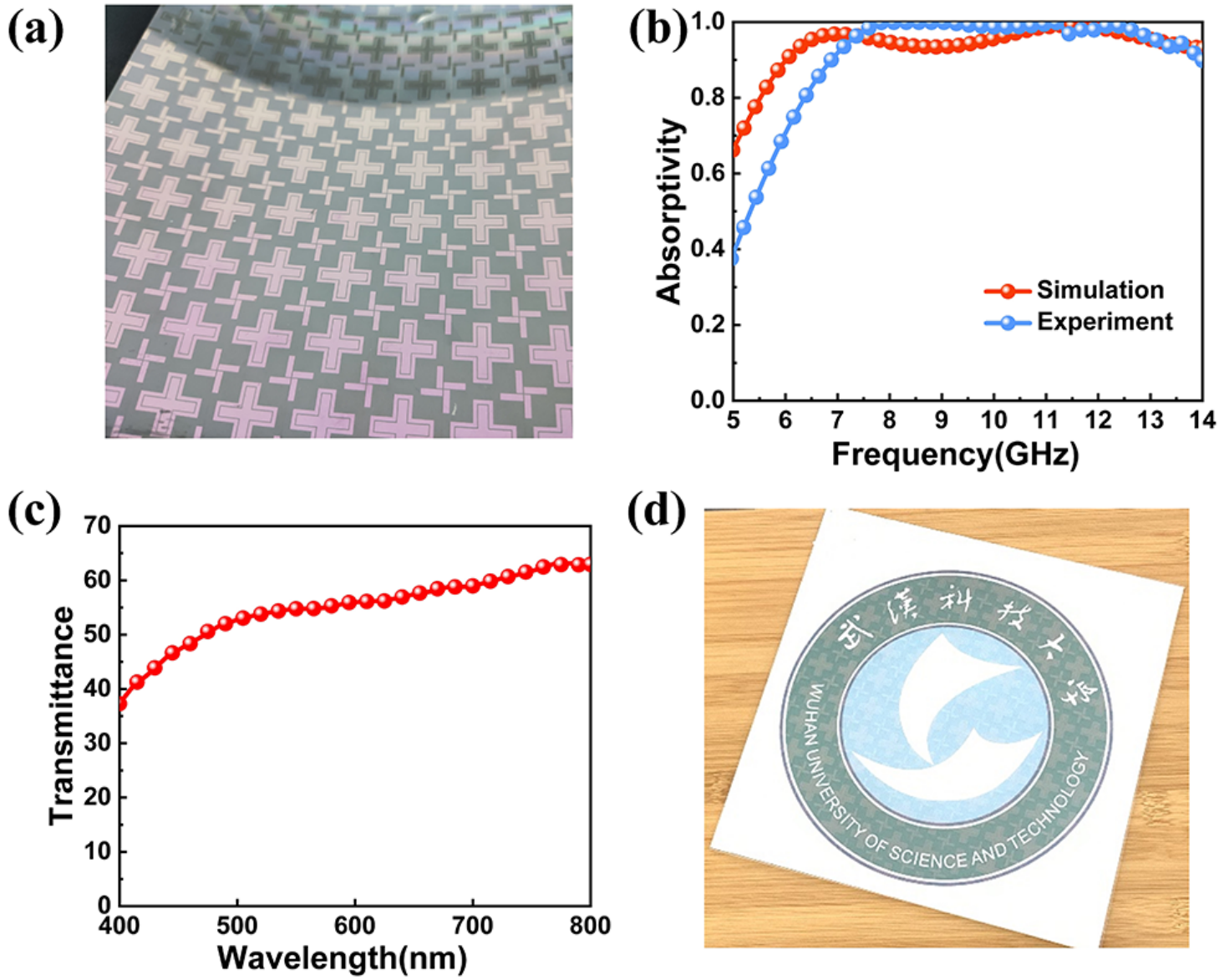

Figure 7

(a) Fabricated transparent MMA, (b) Comparisons of the absorbance between the experimental and simulated results under normal incident EM waves, (c) The measured transmittance curve of the absorber sample, (d) The proposed transparent MMA placed on the emblem of Wuhan University of Science and Technology.

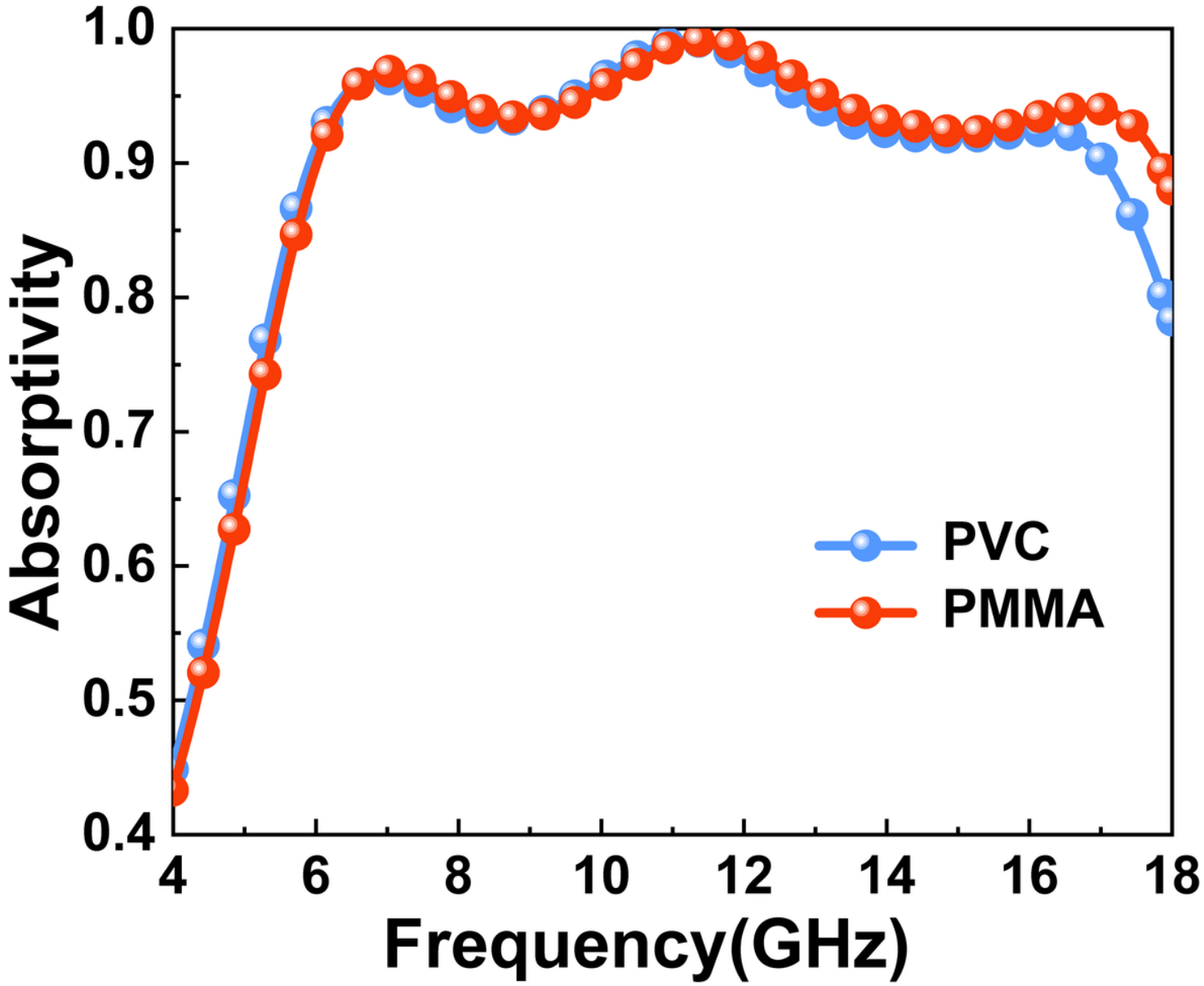

Figure 8

Simulated absorbance curve of using PMMA and PVC media.